Regular Article

PHYSICAL CHEMISTRY RESEARCH
Published by the
Iranian Chemical Society
www.physchemres.org
info@physchemres.org

Phys. Chem. Res., Vol. 9, No. 1, 17-30, March 2021
DOI: 10.22036/pcr.2020.233844.1781

Kinetic, Isotherm, and Thermodynamic Studies of Methylene Blue Adsorption over Metal-doped Zeolite Nano-adsorbent

H. Adel Niaei[a,b], M. Rostamizadeh[a,b,*], F. Maasumi[a,b] and M.J. Darabi[c]

[a]*Faculty of Chemical Engineering, Sahand University of Technology, Sahand New Town, Tabriz, Iran, P. O. Box: 51335-1996*

[b]*Research Center of Environmental Engineering, Sahand University of Technology, Sahand New Town, Tabriz, Iran, P. O. Box: 51335-1996*

[c]*Arkema Inc, 900 First Avenue, King of Prussia, PA, 19406, USA*

(Received 3 June 2020, Accepted 13 September 2020)

In this work, the adsorption of cationic dye by the modified high silica zeolite nano-adsorbent was investigated. The support was prepared hydrothermally and doped by the iron. The morphology, structure, and textural properties of the nano-adsorbents were characterized using XRD, FT-IR, N_2 adsorption-desorption, and FE-SEM. The results showed that the nano-adsorbent had a high specific surface area, crystallinity, and pore volume. The maximum adsorption (6.09 mg g^{-1}) was at the pH level of 9.0, 10 mg l^{-1} of dye concentration, T = 25 °C, and 1.0 g l^{-1} of nano-adsorbent dosage. The kinetic of Methylene blue (MB) adsorption followed the pseudo-second-order with the high correlation factor (R^2 = 0.99). The MB adsorption was in line with the Langmuir model, as an exothermic and spontaneous process. The results confirmed that the metal-doped high silica ZSM-5 zeolite was an efficient nano-adsorbent for the cationic dye adsorption through wastewater treatment.

Keywords: Adsorption, Kinetic, Isotherm, Metal doped, Nano-adsorbent

INTTRODUCTION

Dyes are common organic compounds that can be found in the effluents of leather and textile industries. Methylene blue (MB) as a cationic dye leads to the high heart rate, vomiting, jaundice, shock, and tissue necrosis in humans [1]. The various methods of dye removal include membrane separations [2,3], reverse osmosis [4], Fenton process [5,6], coagulation, and flocculation [7]. Adsorption, as a surface phenomenon, is an easy, low cost, and efficient wastewater treatment method [8,9]. Several nano-adsorbent such as activated carbon [10,11], rice husk [12], peanut shells [13], silica [14], natural zeolites [15,16], and sepiolite [17] have been investigated to remove dye. Auta *et al.* [18] compared the sorption kinetics of MB by raw (RBC) and modified ball clay (MBC). Borah *et al.* [19] reported the adsorption of MB and eosin yellow by carbon, including adsorption capacity 402.25 mg g^{-1} and 400 mg g^{-1}, respectively. Chang *et al.* [20] reported the adsorption of MB over Fe_3O_4/activated montmorillonite (Fe_3O_4/Mt) nano-composite, including the 99.4% removal at reaction conditions of pH = 7.37, 0.5 g of Fe_3O_4/Mt nano-composite, T = 293 K, and 120 mg l^{-1} of MB concentration. Jafari-zare *et al.* [21] reported the adsorption of MB by natural zeolite, including adsorption capacity of 7.9 × 10^{-5} mol g^{-1}. Wang *et al.* [22] reported the removal of MB by polyaniline/TiO_2 (PANI/TiO_2) hydrate with the adsorption capacity of 485.10 mg g^{-1}. Theydan *et al.* [23] studied the removal of MB using biomass-based activated carbon at reaction conditions of pH = 7, 0.5 g l^{-1} of adsorbent dosage, and 4.5 h, leading to the adsorption capacity of 259.25 mg g^{-1}. Setiabudi *et al.* [24] investigated the adsorption of MB over oil palm leaves (OPL) at optimum conditions of pH 6.0, 259 mg l^{-1} of dye, T = 53 °C, and

*Corresponding author. E-mail: Rostamizadeh@sut.ac.ir

2.22 g l^{-1} of adsorbent dosage in which the removal of 88.72% MB was reached. Yousef *et al.* [25] studied the natural zeolite as an adsorbent for phenol removal. They found that the adsorption isotherms were in the following order: Freundlich > Redlich-Peterson > Langmuir > Temkin. Marrakchi *et al.* [26] investigated the adsorption of MB using mesoporous-activated carbon prepared from chitosan flakes (CSAC). They found that the adsorption isotherm was inconsistent with the Langmuir model (q_{max} = 143.53 mg g^{-1}) at 50 °C. It is accepted that ZSM-5 zeolite has the appropriate textural properties for the adsorption process. In this study, ZSM-5 nano-adsorbent, including Fe promoter, was synthesized and applied for the MB adsorption.

EXPERIMENTAL

Materials

The reagents were tetra propyl ammonium bromide, iron nitrate, sodium hydroxide, silicic acid, ammonium nitrate, sodium aluminate, and sulfuric acid, delivered by Merck Company (Germany).

Synthesis

The high silica zeolite support (ZSM-5) synthesis was carried out hydrothermally, including a Si/Al ratio of 200. The detailed procedure of the synthesis is in our previous report [5]. The molar composition of the synthesis solution was $20SiO_2$:$0.05Al_2O_3$:3TPABr:$1.5Na_2O$:$200H_2O$. The crystallization of zeolite was at 180 °C for 48 h. The powder was passed filtration, washing, drying, and calcination (530 °C and 24 h). The iron doping of zeolite support was performed by dissolving the iron source in distilled water (75 ml) and adding to the support. The mixture was stirred for 3h. Then, the modified zeolite was dried and calcined at 530 °C overnight. The metal-doped nano-adsorbent had 1 wt.% Fe species.

Nano-adsorbent Characterization

The nano-adsorbent was characterized by Fourier-transform infrared spectroscopy (FT-IR) analysis with Nexus Model Infrared Spectrophotometric (Nicolet Co, USA) in the range of 400-4000 cm^{-1}. X-ray powder diffraction (XRD) of zeolites was performed on a D8 Advance Bruker AXS X-ray diffractometer using Ni-filtered Cu Kα radiation (λ = 0.15418 nm). The morphology and chemical analysis were determined using field-emission scanning electron microscopy (FE-SEM) by a KYKY (Model, EM3200). The N_2 adsorption-desorption technique was measured at -196.2 °C (Quantachrome, USA). The total surface area (S_{BET}) and total volume (V_{meso}) were determined by the Brunauer-Emmet-Teller (BET) isothermal equation and the pore diameter were estimated by BJH desorption. The t-plot method calculates the micropore volume (V_{micro}). The mesopore volume (V_{meso}) is difference of the calculated total data and the corresponding micropore data. The point of zero charge (pH_{pzc}) of nano-adsorbent was determine using the conventional method (Kalhori *et al.*, 2013). Firstly, the initial pH value of different solutions (0.1 l of 0.1 M NaCl) was adjusted in a pH range of 2-7 by 1 M HCl or NaOH solution. Then, 1.0 g of the nano-adsorbent was added to each solution and stirred for 48 h. Finally, the pH of solution was measured. The value of pH_{pzc} of nano-adsorbent was found from the intersection of the curve of final *vs.* initial pH.

Adsorption Procedure

The adsorption of MB in the batch system was conducted over the modified nano-adsorbent. The experiments of adsorption kinetic were conducted by adding 3.0 g l^{-1} of the nano-adsorbent in 50 ml MB solution (10 mg l^{-1}) at pH = 9.0. HCl or NaOH (0.1 M) adjusted the solution pH. After the adsorption experiments, the residual concentration of MB in the solution was determined by a Jenway 6705 UV-Vis spectrophotometer (England). The removal efficiency and the adsorption value (q_t) were obtained as the following:

$$\text{Re}moval\ (\%) = \frac{C_0 - C_t}{C_0} \times 100 \quad (1)$$

$$q_e = \frac{C_0 - C_e}{m} \times V \quad (2)$$

where C_0 and C_e (mg l^{-1}) were the concentrations at initial and equilibrium, respectively. q_e (mg g^{-1}) is the adsorbed value. C_t (mg l^{-1}) is the concentration of MB at time t, V (l) is the volume and m (g) is the nano-adsorbent mass.

RESULTS AND DISCUSSION

Characterization

The FT-IR spectra of the nano-adsorbent are depicted in Fig. 1. The rings of zeolite with 5 members result in the band at 550 cm^{-1}. The band at around 3680 cm^{-1} can be attributed to the Al-OH group in the zeolite. The FT-IR spectra at 3610 cm^{-1} and 3680 cm^{-1} are assigned to Si-OH-Al [27-29]. The XRD results confirm the correct synthesis of the HZSM-5 zeolite with the high crystallinity (Fig. 2). The XRD pattern of the modified zeolite is similar to the parent, indicating no change of the structure through the impregnation process.

Furthermore, there is no peak associated with the Fe promoter indicating the uniform distribution of Fe promoter in the ZSM-5 structure. The textural data of the parent and modified zeolites are shown in Table 1. The BET surface area is 321.1 and 291.8 m^2 g^{-1} for the parent and modified nano-adsorbent, respectively. The decrease in pore volume and surface area of the modified nano-adsorbent can be explained by the pore blockage owing to iron species [30]. The isotherms are type IV based on IUPAC classification (Fig. 3). Uptake at low pressures indicates the microporous structure [5,31]. After the impregnation, the morphology and distribution of the particle size of the parent and modified nano-adsorbent do not change significantly (Fig. 4).

Effect of Solution pH

Figure 5 represents the MB adsorption on the modified nano-adsorbent at different initial pHs. The adsorption of MB strongly depends on the solution pH. The increase in the pH from 3.0 to 9.0 leads to the high adsorption of MB. The maximum adsorption capacity is obtained at pH of 9.0 (3.248 mg g^{-1}) within 96 min. The results can be explained by the electrostatic effects. The pH value at the point of zero charge (pH_{pzc}) for the nano-adsorbent was equal to 4. The surface of the nano-adsorbent is protonated at pH < pH_{pzc}, which causes electrostatic repulsions with MB molecules. At higher pH values (pH > pH_{pzc}), stronger electrostatic attraction is created between the positive charged MB molecules (pKa = 3.8) and negatively charged surface of the nano-adsorbent [32,33]. Therefore, the adsorption capacity is increased.

Effect of Nano-adsorbent Dosage

The effect of various amounts of the parent and modified nano-adsorbent on the adsorption of MB are shown in Fig. 6. The adsorbent amount significantly influences the adsorption of MB dye. For both adsorbents, the adsorption capacity decreases with increasing the adsorbent amount [34]. It can be explained by the saturation of sites over MB molecules, and, or the solid aggregation as a result of particle-particle interaction. The modified nano-adsorbent has a higher adsorption capacity than the parent zeolite for the adsorption of MB. The use of Fe for the modification of the parent nano-adsorbent improves its characteristics to adsorption of more MB.

Effect of MB Concentration

Figure 7 depicts the MB removal change by the dye concentration. It is clear that the adsorption is decreased by the increase of the initial concentration from 10 to 20 mg l^{-1} at operating conditions of pH 9.0, 3.0 g l^{-1} of the modified nano-adsorbent dosage, and T = 25 °C. At the high concentration, the active sites of the nano-adsorbent are saturated by the dye molecules [35,36] and so the removal of MB drops. However, the adsorption capacity is increased from 3.29 to 4.49 mg g^{-1} with the increase of the initial concentration (Fig. 8). The increase in the adsorption capacity is due to the high driving force of mass transfer and the high rate of adsorption between the aqueous and solid phases [37,38].

Effect of temperature. Figure 9 represents the efficiency of the modified nano-adsorbent at different temperatures. The adsorption capacity of MB decreases from 3.25 mg g^{-1} to 2.94 mg g^{-1} within 96 min when temperature increases from 25 °C to 35 °C in operating conditions of C_0 = 10 mg l^{-1}, pH = 9.0 and 3.0 g l^{-1} of nano-adsorbent. The results indicate the MB adsorption as an exothermic process. Bakhelkha *et al.* [39] reported that the decreased adsorption of amoxicillin with temperature increasing from 25 to 50 °C was attributed to the weak forces between the adsorbent and adsorbate at high temperatures.

Adsorption Isotherms

Various isotherm equations such as Langmuir [40], Freundlich [41] and Temkin [34] were studied to clarify the

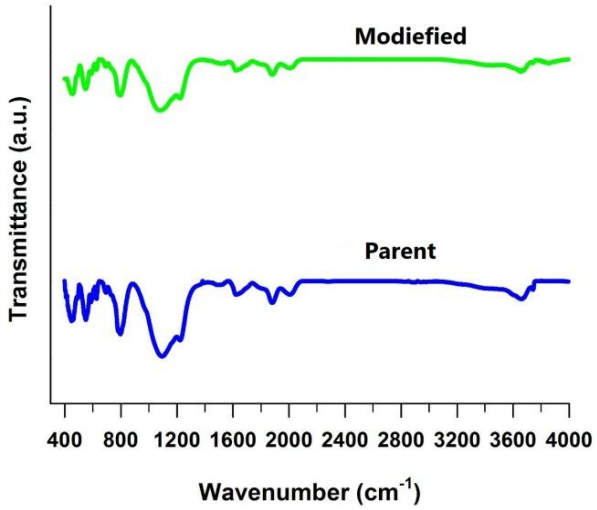

Fig. 1. FT-IR spectra of the parent and modified nano-absorbent.

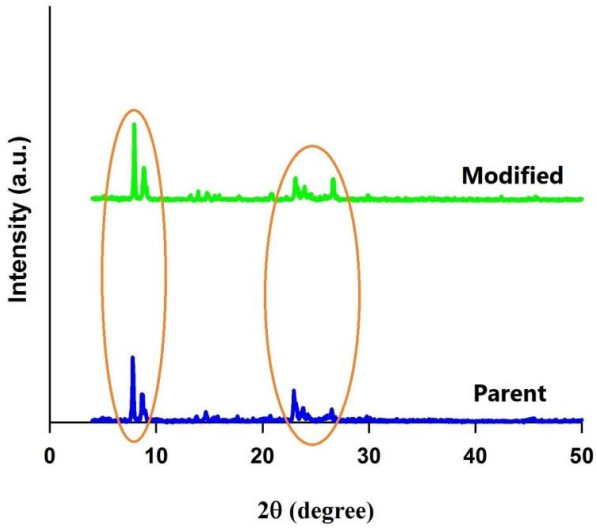

Fig. 2. The XRD pattern of the parent and modified nano-absorbent.

Table 1. Crystallinity and Textural Data of the Parent and Modified Adsorbent

Adsorbent	Crystallinity (%)	S_{BET} ($m^2 g^{-1}$)	V_{total} ($cm^3 g^{-1}$)	V_{micro} ($cm^3 g^{-1}$)	V_{meso} ($cm^3 g^{-1}$)
Parent	100.00	321.10	0.19	0.13	0.06
Modified	81.28	291.80	0.17	0.11	0.06

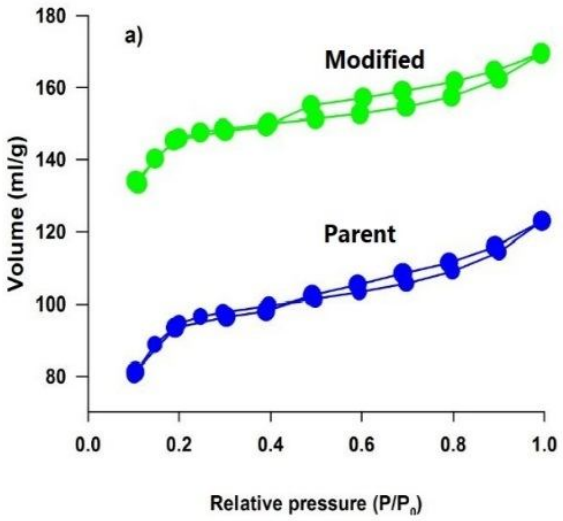

Fig. 3. N_2 adsorption-desorption isotherm for the parent and modified nano-absorbent.

adsorption mechanism of MB molecules on the high silica iron-doped nano-adsorbent. The linear forms of equations are given as follows:

$$\frac{C_e}{q_e} = \frac{1}{K_L\, q_{\max}} + \frac{C_e}{q_{\max}} \tag{3}$$

$$\ln q_e = \ln k_f + \frac{1}{n}\ln C_e \tag{4}$$

$$q_e = B_T \ln A_T + B_T \ln C_e \qquad , B_T = \frac{RT}{b_T} \tag{5}$$

where C_e is the equilibrium concentration, q_e is the adsorbed dye, K_L is the Langmuir constant and q_{max} is the maximum capacity. k_f and 1/n are the constant Freundlich isotherm, showing capacity and intensity of the adsorption over the nano-adsorbent, respectively. b_T is the variation of adsorption energy, A_T is binding equilibrium, and C_e is equilibrium dye concentration. Furthermore, the separation factor (R_L) is calculated by Eq. (6).

$$R_L = \frac{1}{1 + K_L C_i} \tag{6}$$

where C_i is the initial MB concentration. It is reported that the adsorption is favorable if $0 < R_L < 1$ [20,42]. The calculated results for the isotherm models are listed in Table 2. Langmuir model is the well-fitted ($R^2 = 0.99$) for the MB adsorption (Fig. 10). The highest monolayer MB adsorption capacity (q_{max} = 4.56 mg g^{-1}) was in a better agreement with the experimental data ($q_{e,cal}$ = 4.48 mg g^{-1}). Moreover, the separation factor (R_L = 0.015) is in the range of $0 < R_L < 1$, revealing the favorable adsorption.

Adsorption Kinetic

The adsorption kinetic is investigated using the pseudo-second-order model (Eq. (7)).

$$\frac{t}{q_t} = \frac{1}{k_2 q_e^2} + \frac{t}{q_e} \tag{7}$$

where k_2 is the second-order rate coefficient, the fitting results for the pseudo-second-order kinetic are displayed in Fig. 11 and Table 3. The pseudo-second-order kinetic exhibited a good agreement with adsorption data ($R^2 > 0.99$).

Thermodynamic Study

The adsorption thermodynamic is studied to describe the adsorption behaviors. The thermodynamic factors, such as standard entropy (ΔS°), standard free energy (ΔG°), and standard enthalpy (ΔH°), are determined as follows: [43].

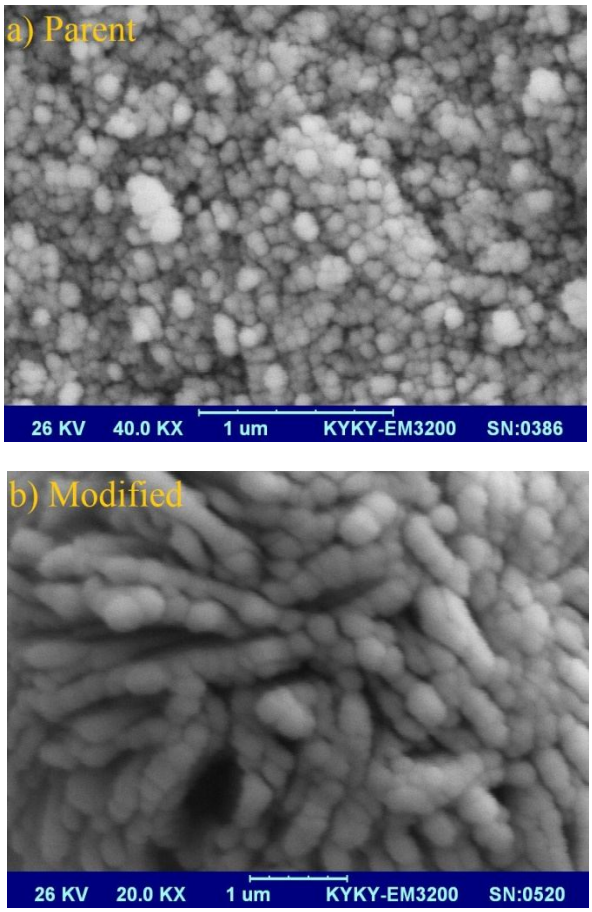

Fig. 4. FE-SEM image of the (a) parent, and (b) modified nano-adsorbent.

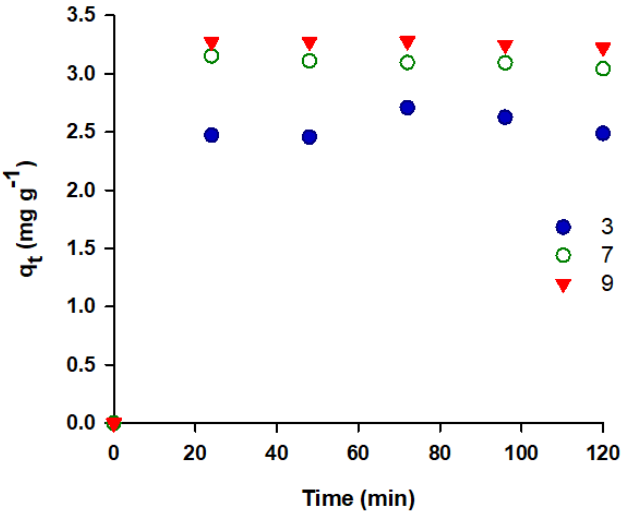

Fig. 5. Effect of solution pH on the adsorption. Operating conditions: 10 mg l^{-1} of initial concentration, T = 25 °C, and 3.0 g l^{-1} of the modified nano-adsorbent.

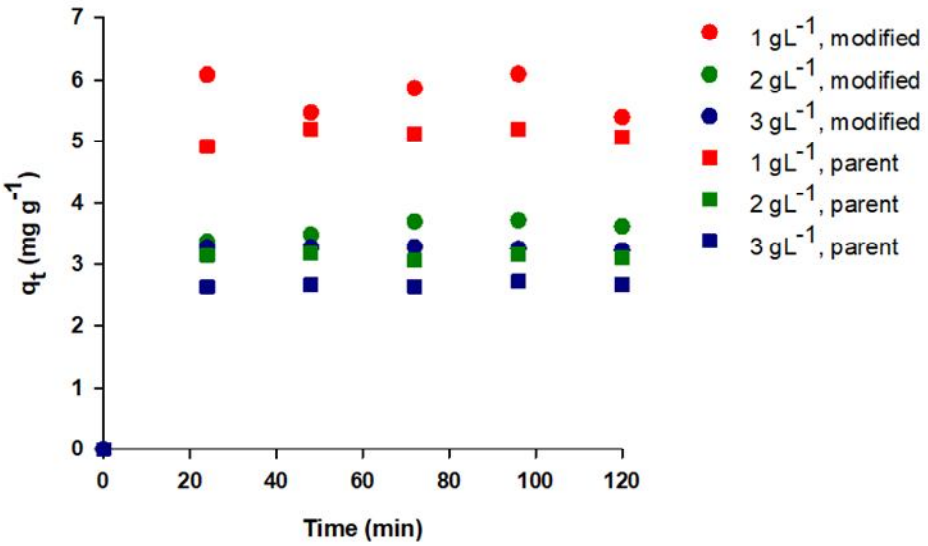

Fig. 6. Effect of the parent and modified nano-adsorbent dosage on adsorption. Operating conditions: pH = 9.0, T = 25 °C, and 10 mg l^{-1} of initial concentration.

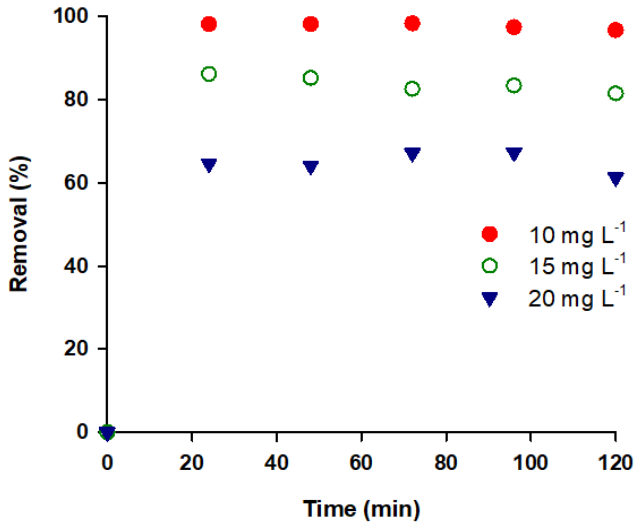

Fig. 7. Effect of the initial MB concentration on adsorption. Operating conditions: pH = 9.0, T = 25 °C, and 3.0 g l^{-1} of nano-adsorbent dosage.

$$\Delta G^\circ = -RT \ln K_C \quad (8)$$

$$\ln K_C = \ln K_L = \frac{-\Delta G^\circ}{RT} \quad (9)$$

$$\ln K_L = \frac{\Delta G^\circ}{R} - \frac{\Delta H^\circ}{RT} \quad (10)$$

$$\Delta G^\circ = \Delta H^\circ - T\Delta S^\circ \quad (11)$$

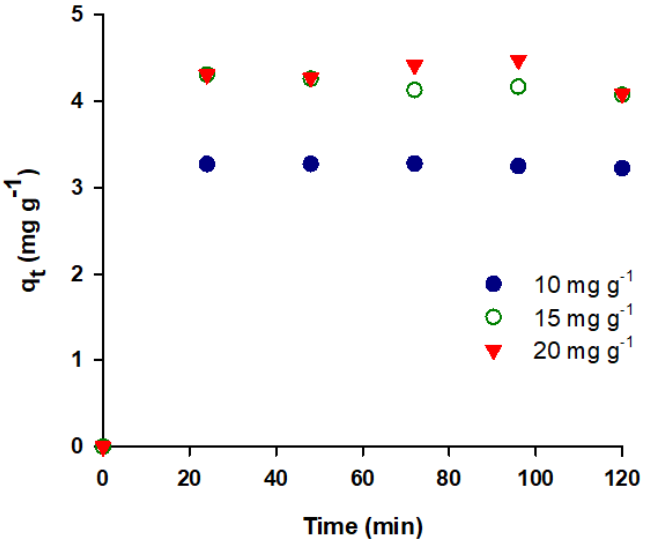

Fig. 8. Effect of the initial MB concentration on adsorption. Operating conditions: pH = 9.0, T = 25 °C, and 3.0 g l^{-1} of nano-adsorbent dosage.

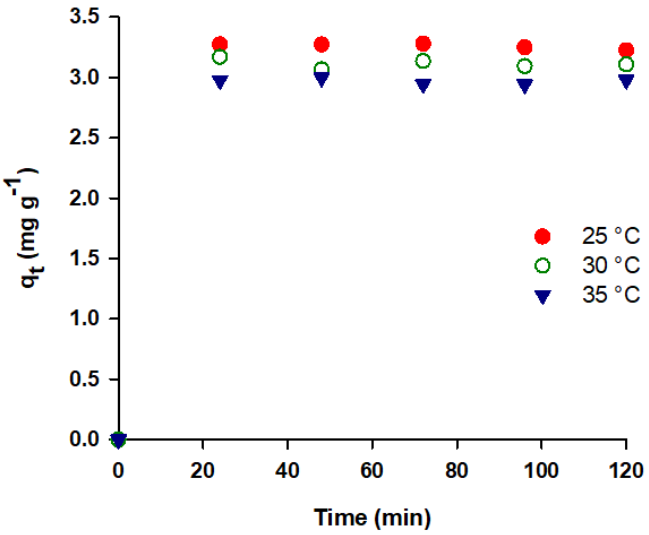

Fig. 9. Effect of the solution temperature of MB on adsorption. Operating conditions: pH = 9.0, C_0 = 10 mg l^{-1} and 3.0 g l^{-1} of nano-adsorbent dosage.

where K_c is equal to K_L (Langmuir constant), and R (8.314 J mol^{-1} K^{-1}) is the gas constant universal. According to Eq. (10), ΔH° and ΔS° can be obtained from the slope and intercept of the linear plot lnK_L *vs*. 1/T. The thermodynamic parameters for the MB adsorption are shown in Table 4. The negative ΔH˙ reveals that the MB adsorption on the nano-adsorbent is exothermic. The negative ΔG° demonstrates that the MB adsorption is a

Table 2. Isotherm Data for the Adsorption of MB

Isotherm models	Temperature (°C)	Parameters isotherm	
Langmuir	25	q_{max} (mg g^{-1})	4.56
		$q_{e,cal}$ (mg g^{-1})	4.48
		K_L (l mg^{-1})	6.51
		R^2	0.99
Freundlich	25	K_f ((mg g^{-1}) (l $mg^{-1})^{1/n}$)	3.74
		1/n	0.10
		R^2	0.99
Temkin	25	A_T (M^{-1})	19535.72
		b_T (kJ mol^{-1})	6.47
		R^2	0.99

Table 3. Kinetic Data of the MB Adsorption

Parameters	$q_{e,cal}$ (mg g^{-1})	Pseudo-Second-Order		
		$q_{e,exp}$ (mq q^{-1})	k_2 (g mg^{-1} min^{-1})	R^2
C_0 (mg l^{-1})				
10	3.25	3.23	0.80	0.99
15	4.17	4.08	0.25	0.99
20	4.48	4.21	0.21	0.99
M (modified, g l^{-1})				
1	6.09	5.59	0.14	0.99
2	3.71	3.68	0.02	0.99
3	3.25	3.23	0.80	0.99
M (parent, g l^{-1})				
1	5.20	5.11	0.76	0.99
2	3.16	3.12	2.28	0.99
3	2.72	2.69	1.18	0.99
pH				
3	2.63	2.55	3.46	0.99
7	3.09	3.05	0.54	0.99
9	3.25	3.23	0.80	0.99
T (°C)				
25	3.25	3.23	0.80	0.99
30	3.09	3.10	2.93	0.99
35	2.94	2.96	7.87	0.99

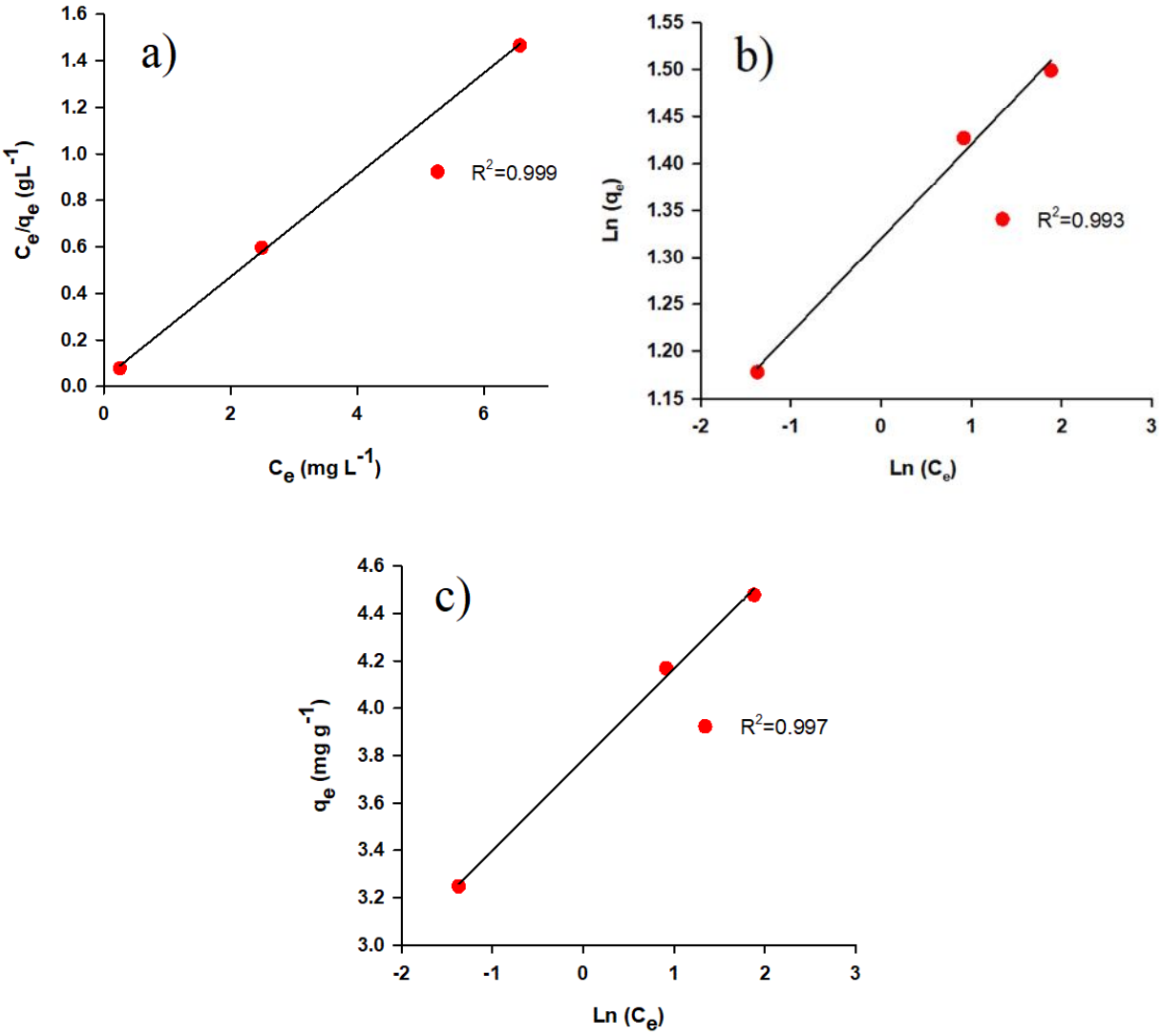

Fig. 10. (a) Langmuir, (b) Freundlich, and (c) Temkin isotherms for MB removal.

Table 4. Langmuir and Thermodynamic Parameters for the MB Adsorption

Langmuir parameter	25 (°C)	30 (°C)	35 (°C)
K_L (l mg^{-1})	6.51	5.65	5.47
R^2	0.99	0.99	0.99
$\Delta G°$(kJ K mol^{-1})	-27.24		
$\Delta H°$ (kJ K mol^{-1})	-12723.08		
$\Delta S°$(kJ K mol^{-1} K^{-1})	-46.50		

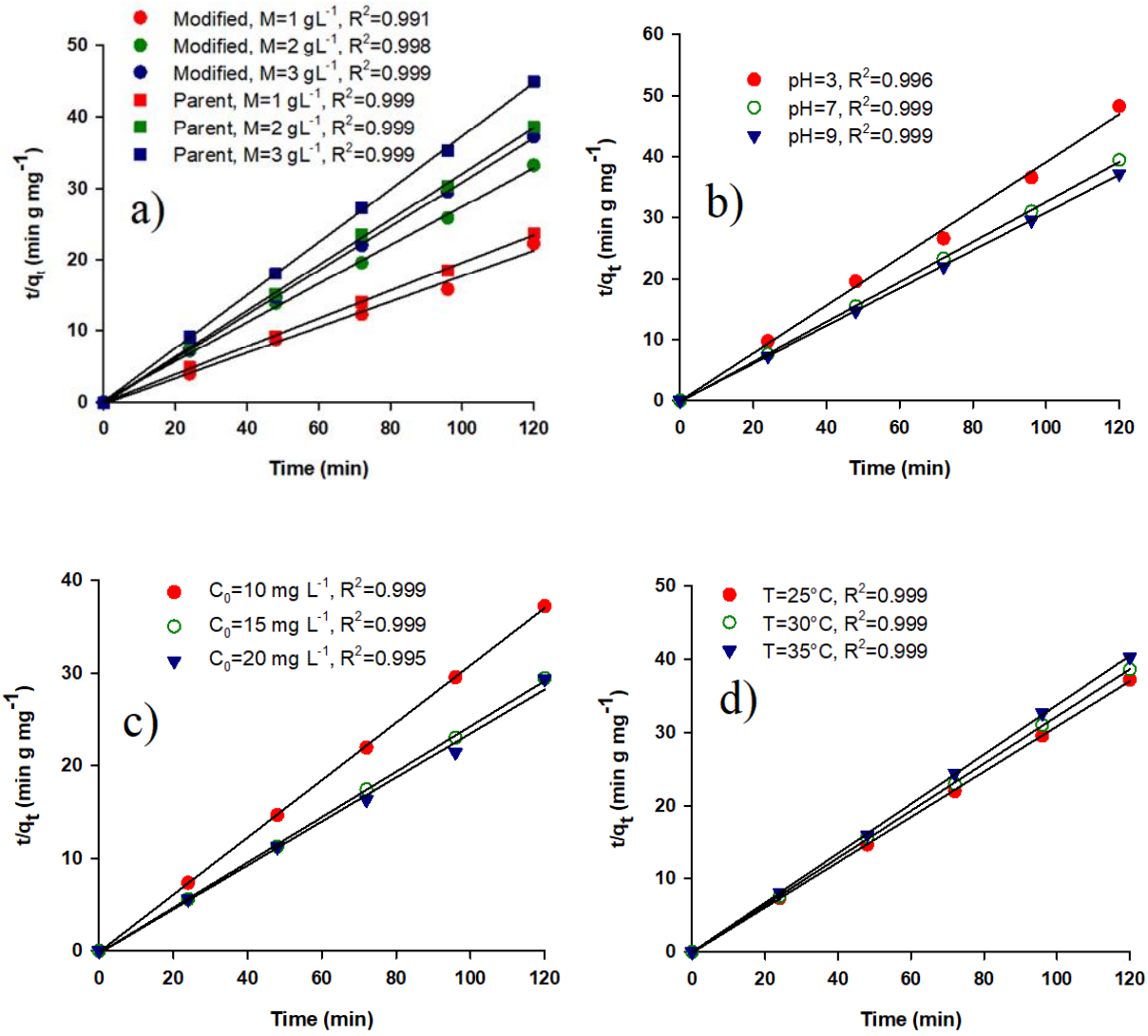

Fig. 11. Pseudo-second-order kinetic for the MB adsorption at different (a) adsorbent dosages (b) pH levels (c) initial concentrations (d) temperatures.

spontaneously favorable process. The negative ΔS° confirms the reduction in randomness at the solid-solution interface and no significant changes in the internal structure of adsorbent for the MB adsorption.

CONCLUSION

The high silica iron-doped ZSM-5 nano-adsorbent was prepared and applied for the MB adsorption. The modified nano-adsorbent had a high surface area, spherical morphology, and uniform distribution of Fe promoter. The results showed that the Langmuir model was in consistent with the experimental data (R^2 = 0.99 and q_{max} = 4.56). The kinetic of the MB adsorption followed the pseudo-second-order model (R^2 = 0.99). The optimum operating conditions for the MB adsorption were pH of 9.0, 1.0 g l^{-1} of the nano-adsorbent dosage, T = 25 °C, and 10 mg l^{-1} of MB concentration, which resulted in the adsorption capacity of 6.09 mg g^{-1} for the modified nano-adsorbent. The thermodynamic properties indicated an exothermic and

spontaneous process. Therefore, the results of this study revealed that modified zeolite could be a high efficient nano-adsorbent for the MB adsorption from the aqueous solutions.

REFERENCES

[1] Gharibian, S.; Hazrati, H.; Rostamizadeh, M., Continuous electrooxidation of Methylene Blue in filter press electrochemical flowcell: CFD simulation and RTD validation. *Chemical Engineering and Processing-Process Intensification* **2020**, *150*, 107880, DOI: 10.1016/j.cep.2020.107880..

[2] Behboudi, A.; Jafarzadeh, Y.; Yegani, R., Polyvinyl chloride/polycarbonate blend ultrafiltration membranes for water treatment. *J. Membr. Sci.* **2017**, *534*, 18-24, DOI: 10.1016/j.memsci.2017.04.011.

[3] Hazrati, H.; Jahanbakhshi, N.; Rostamizadeh, M., Fouling reduction in the membrane bioreactor using synthesized zeolite nano-adsorbents. *J. Membr. Sci.* **2018**, *555*, 455-462, DOI: 10.1016/j.memsci.2018.03.076.

[4] Malaeb, L.; Ayoub, G. M., Reverse osmosis technology for water treatment: state of the art review. *Desalination* **2011**, *267*, 1-8, DOI: 10.1016/j.desal.2010.09.001.

[5] Rostamizadeh, M.; Jafarizad, A.; Gharibian, S., High efficient decolorization of reactive red 120 azo dye over reusable Fe-ZSM-5 nanocatalyst in electro-Fenton reaction. *Sep. Purif. Technol.* **2018**, *192*, 340-347, DOI: 10.1016/j.seppur.2017.10.041.

[6] Vosoughi, M.; Fatehifar, E.; Derafshi, S.; Rostamizadeh, M., High efficient treatment of the petrochemical phenolic effluent using spent catalyst: Experimental and optimization. *J. Enviro. Chem. Eng.* **2017**, *5*, 2024-2031, DOI:10.1016/j.jece.2017.04.003.

[7] Verma, A. K.; Dash, R. R.; Bhunia, P., A review on chemical coagulation/flocculation technologies for removal of colour from textile wastewaters. *J. Environ. Manage.* **2012**, *93*, 154-168, DOI: 10.1016/j.jenvman.2011.09.012.

[8] Salehi, A.; Najafi Kani, E., Green cylindrical mesoporous adsorbent based on alkali-activated phosphorous slag: synthesis, dye removal, and RSM modeling. *Adsorption* **2018**, *24*, 647-666, DOI: 10.1007/s10450-018-9972-z.

[9] Khenifi, A.; Bouberka, Z.; Sekrane, F.; Kameche, M.; Derriche, Z., Adsorption study of an industrial dye by an organic clay. *Adsorption* **2007**, *13*, 149-158, DOI: 10.1007/s10450-007-9016-6.

[10] Gil, A.; Santamaría, L.; Korili, S. A., Removal of caffeine and diclofenac from aqueous solution by adsorption on multiwalled carbon nanotubes. *Colloid. Interfac. Sci.* **2018**, *22*, 25-28, DOI: 10.1016/j.colcom.2017.11.007.

[11] Hassan, A. F.; Elhadidy, H., Effect of Zr^{+4} doping on characteristics and sonocatalytic activity of TiO2/carbon nanotubes composite catalyst for degradation of chlorpyrifos. *J. Phys. Chem. Solids* **2019**, *129*, 180-187, DOI: 10.1016/j.jpcs.2019.01.018.

[12] Bhatti, H. N.; Jabeen, A.; Iqbal, M.; Noreen, S.; Naseem, Z., Adsorptive behavior of rice bran-based composites for malachite green dye: isotherm, kinetic and thermodynamic studies. *J. Mol. Liq.* **2017**, *237*, 322-333, DOI: 10.1016/j.molliq.2017.04.033.

[13] Georgin, J.; Dotto, G. L.; Mazutti, M. A.; Foletto, E. L., Preparation of activated carbon from peanut shell by conventional pyrolysis and microwave irradiation-pyrolysis to remove organic dyes from aqueous solutions. *J. Enviro. Chem. Eng.* **2016**, *4*, 266-275, DOI: 10.1016/j.jece.2015.11.018.

[14] Dominguez, M. A.; Etcheverry, M.; Zanini, G. P., Evaluation of the adsorption kinetics of brilliant green dye onto a montmorillonite/alginate composite beads by the shrinking core model. *Adsorption* **2019**, *25*, 1387-1396, DOI: 10.1007/s10450-019-00101-w.

[15] Mouni, L.; Belkhiri, L.; Bollinger, J.-C.; Bouzaza, A.; Assadi, A.; Tirri, A.; Dahmoune, F.; Madani, K.; Remini, H., Removal of methylene blue from aqueous solutions by adsorption on kaolin: Kinetic and equilibrium studies. *Appl. Clay Sci.* **2018**, *153*, 38-45, DOI: 10.1016/j.clay.2017.11.034.

[16] Rios, A. G.; Matos, L. C.; Manrique, Y. A.; Loureiro, J. M.; Mendes, A.; Ferreira, A. F. P., Adsorption of anionic and cationic dyes into shaped MCM-41. *Adsorption* **2020**, *26*, 75-88, DOI: 10.1007/s10450-019-00176-5.

[17] Demirbaş, Ö.; Turhan, Y.; Alkan, M.,

Thermodynamics and kinetics of adsorption of a cationic dye onto sepiolite. *Desalin. Water Treat.* **2015**, *54*, 707-714, DOI: 10.1080/19443994.2014.886299.

[18] Auta, M.; Hameed, B., Modified mesoporous clay adsorbent for adsorption isotherm and kinetics of methylene blue. *Chem. Eng. J.* **2012**, *198*, 219-227, DOI: 10.1016/j.cej.2012.05.075.

[19] Borah, L.; Goswami, M.; Phukan, P., Adsorption of methylene blue and eosin yellow using porous carbon prepared from tea waste: adsorption equilibrium, kinetics and thermodynamics study. *J. Enviro. Chem. Eng.* **2015**, *3*, 1018-1028, DOI: 10.1016/j.jece.2015.02.013.

[20] Chang, J.; Ma, J.; Ma, Q.; Zhang, D.; Qiao, N.; Hu, M.; Ma, H., Adsorption of methylene blue onto Fe3O4/activated montmorillonite nanocomposite. *Appl. Clay Sci.* **2016**, *119*, 132-140, DOI: 10.1016/j.clay.2015.06.038.

[21] Jafari-zare, F.; Habibi-yangjeh, A., Competitive adsorption of methylene blue and rhodamine B on natural zeolite: thermodynamic and kinetic studies. *Chin. J. Chem.* **2010**, *28*, 349-356, DOI: 10.1002/cjoc.201090078.

[22] Wang, N.; Chen, J.; Wang, J.; Feng, J.; Yan, W., Removal of methylene blue by Polyaniline/TiO_2 hydrate: Adsorption kinetic, isotherm and mechanism studies. *Powder Technol.* **2019**, *347*, 93-102, DOI: 10.1016/j.powtec.2019.02.049.

[23] Theydan, S. K.; Ahmed, M. J., Adsorption of methylene blue onto biomass-based activated carbon by FeCl3 activation: Equilibrium, kinetics, and thermodynamic studies. *J. Anal. Appl. Pyrolysis* **2012**, *97*, 116-122, DOI: 10.1016/j.jaap.2012.05.008.

[24] Setiabudi, H.; Jusoh, R.; Suhaimi, S.; Masrur, S., Adsorption of methylene blue onto oil palm (Elaeis guineensis) leaves: Process optimization, isotherm, kinetics and thermodynamic studies. *J. Taiwan Inst. Chem. Eng.* **2016**, *63*, 363-370, DOI: 10.1016/j.jtice.2016.03.035.

[25] Yousef, R. I.; El-Eswed, B.; Ala'a, H., Adsorption characteristics of natural zeolites as solid adsorbents for phenol removal from aqueous solutions: Kinetics, mechanism, and thermodynamics studies. *Chem. Eng. J.* **2011**, *171*, 1143-1149, DOI: 10.1016/j.cej.2011.05.012.

[26] Marrakchi, F.; Ahmed, M.; Khanday, W.; Asif, M.; Hameed, B., Mesoporous-activated carbon prepared from chitosan flakes *via* single-step sodium hydroxide activation for the adsorption of methylene blue. *Int. J. Biol. Macromol.* **2017**, *98*, 233-239, DOI: 10.1016/j.ijbiomac.2017.01.119.

[27] Rostamizadeh, M.; Taeb, A., Synthesis and characterization of HZSM-5 catalyst for methanol to propylene (MTP) reaction. *Synth. React. Inorg., Met.-Org., Nano-Met. Chem.* **2016**, *46*, 665-671, DOI: 10.1080/15533174.2014.988825.

[28] Rostamizadeh, M.; Jalali, H.; Naeimzadeh, F.; Gharibian, S., Efficient removal of diclofenac from pharmaceutical wastewater using impregnated Zeolite catalyst in heterogeneous fenton process. *Phys. Chem. Res.* **2019**, *7*, 37-52, DOI: 10.22036/pcr.2018.144779.1524.

[29] O'malley, A. J.; Parker, S. F.; Chutia, A.; Farrow, M. R.; Silverwood, I. P.; García-Sakai, V.; Catlow, C. R. A., Room temperature methoxylation in zeolites: insight into a key step of the methanol-to-hydrocarbons process. *Chem. Commun.* **2016**, *52*, 2897-2900, DOI: 10.1039/c5cc08956e.

[30] Darabi Mahboub, M. J.; Dubois, J.-L.; Cavani, F.; Rostamizadeh, M.; Patience, G. S., Catalysis for the synthesis of methacrylic acid and methyl methacrylate. *Chem. Soc. Rev.* **2018**, *47*, DOI: 7703-7738, 10.1039/C8CS00117K.

[31] Darabi Mahboub, M. J.; Rostamizadeh, M.; Dubois, J. -L.; Patience, G. S., Partial oxidation of 2-methyl-1,3-propanediol to methacrylic acid: experimental and neural network modeling. *RSC Advances* **2016**, *6*, 114123-114134, DOI: 10.1039/C6RA16605A.

[32] Jung, K. -W.; Choi, B. H.; Hwang, M. -J.; Jeong, T.-U.; Ahn, K. -H., Fabrication of granular activated carbons derived from spent coffee grounds by entrapment in calcium alginate beads for adsorption of acid orange 7 and methylene blue. *Bioresour. Technol.* **2016**, *219*, 185-195, DOI: 10.1016/j.biortech.2016.07.098.

[33] Hammed, A. K.; Dewayanto, N.; Du, D.; Ab Rahim, M. H.; Nordin, M. R., Novel modified ZSM-5 as an

efficient adsorbent for methylene blue removal. *J. Enviro. Chem. Eng*. **2016**, *4*, 2607-2616, DOI: 10.1016/j.jece.2016.05.008.

[34] Fathi, M.; Asfaram, A.; Farhangi, A., Removal of Direct Red 23 from aqueous solution using corn stalks: Isotherms, kinetics and thermodynamic studies. *Spectrochim. Acta, Part A* **2015**, *135*, 364-372, DOI: 10.1016/j.saa.2014.07.008.

[35] Ali, M. M.; Ahmed, M.; Hameed, B., NaY zeolite from wheat (Triticum aestivum L.) straw ash used for the adsorption of tetracycline. *J. Clean. Prod.* **2018**, *172*, 602-608, DOI: 10.1016/j.jclepro.2017.10.180.

[36] Kaur, S.; Rani, S.; Mahajan, R.; Asif, M.; Gupta, V. K., Synthesis and adsorption properties of mesoporous material for the removal of dye safranin: kinetics, equilibrium, and thermodynamics. *J. Ind. Eng. Chem*. **2015**, *22*, 19-27, DOI: 10.1016/ j.jiec.2014.06.019.

[37] Ceylan, Z.; Mustafaoglu, D.; Malkoc, E., Adsorption of phenol by MMT-CTAB and WPT-CTAB: Equilibrium, kinetic, and thermodynamic study. *Part. Sci. Technol.* **2018**, *36*, 716-726, DOI: 10.1080/ 02726351.2017.1296047.

[38] Sun, Y.; Yang, Y.; Yang, M.; Yu, F.; Ma, J., Response surface methodological evaluation and optimization for adsorption removal of ciprofloxacin onto graphene hydrogel. *J. Mol. Liq*. **2019**, *284*, 124-130, DOI: 10.1016/j.molliq.2019.03.118.

[39] Boukhelkhal, A.; Benkortbi, O.; Hamadache, M.; Ghalem, N.; Hanini, S.; Amrane, A., Adsorptive removal of amoxicillin from wastewater using wheat grains: equilibrium, kinetic, thermodynamic studies and mass transfer. *Desalin. Water Treat.* **2016**, *57*, 27035-27047, DOI: 10.1080/ 19443994.2016.1166991.

[40] Silva, T. L.; Cazetta, A. L.; Souza, P. S.; Zhang, T.; Asefa, T.; Almeida, V. C., Mesoporous activated carbon fibers synthesized from denim fabric waste: efficient adsorbents for removal of textile dye from aqueous solutions. *J. Clean. Prod.* **2018**, *171*, 482-490, DOI: 10.1016/j.jclepro.2017.10.034.

[41] Aghdasinia, H.; Asiabi, H. R., Adsorption of a cationic dye (methylene blue) by Iranian natural clays from aqueous solutions: equilibrium, kinetic and thermodynamic study. *Environ. Earth Sci.* **2018**, *77*, 218, DOI: 10.1007/s12665-018-7342-5.

[42] Abbas, M.; Trari, M., Kinetic, equilibrium and thermodynamic study on the removal of congo red from aqueous solutions by adsorption onto apricot stone. *Process Saf. Environ. Prot.* **2015**, *98*, 424-436, DOI: 10.1016/j.psep.2015.09.015.

[43] [43] Tran, H. N.; You, S.-J.; Chao, H.-P., Thermodynamic parameters of cadmium adsorption onto orange peel calculated from various methods: a comparison study. *J. Enviro. Chem. Eng*. **2016**, *4*, 2671-2682, DOI: 10.1016/j.jece.2016.05.009.